agronomy

MDPI

Article

Spatial Patterns and Drivers of Soil Moisture and Infiltration in Abandoned Karst Sloping Farmland

Zhimeng Zhao [1,*] and Jin Zhang [2]

[1] School of Geography and Resources, Guizhou Education University, Guiyang 550018, China
[2] School of Mathematical Sciences, University of the Chinese Academy of Sciences, Beijing 100049, China; zhangj@ucas.ac.cn
* Correspondence: zhaozhimeng@gznc.edu.cn

Abstract

To study the soil moisture dynamics and rainfall infiltration characteristics of karst sloping farmland and their driving factors, an abandoned farmland was selected for this study, and five monitoring points (from the foot, S1, of the slope to the top, S5) were set along the terrain gradient. The volumetric water content data of the 0–40 cm soil layer was obtained through in situ monitoring for one year. The infiltration characteristics were quantified in combination with a staining tracer test, and the soil properties were determined. The results showed that the soil moisture content increased with the deepening of the soil layer, and there was significant slope differentiation. The moisture content in the downhill slopes (S1, S2) was significantly higher than that in the uphill slopes (S4, S5), and the annual average value of S5 was 27.4% lower than that of S1. The moisture difference ($\Delta\theta$, the difference in moisture content between hillslope and flatland) changed from positive to negative from the foot of the slope to the top, indicating that moisture was transported downward along the slope surface. A dye tracer showed that from S1 to S5, the water transport pathway gradually shifted from exhibiting deeper vertical penetration and narrower lateral spread to showing shallower vertical penetration and wider lateral spread. The preferential flow index decreased from 46.6 $\pm$ 2.3% to 34.7 $\pm$ 2.1%, indicating a progressive reduction in rapid vertical channeling, while the lateral flow index reached its peak (21.4 $\pm$ 2.7%) in the middle of the slope (S3), suggesting enhanced horizontal water redistribution at this position. Correlation analysis indicated that soil bulk density was extremely significantly negatively associated with infiltration capacity, while capillary porosity, non-capillary porosity, total porosity, organic matter, and high aggregate content were extremely significantly positively associated with infiltration capacity. These results revealed that the topographic gradient affected soil moisture and water infiltration paths by regulating soil physical properties in this karst forest ecosystem. It should be noted that the research results are only applicable to one slope and should not be directly extended to all karst slope agricultural landscapes.

Keywords: dye tracer; karst hillslope; preferential flow; soil moisture; soil properties

Check for updates

Academic Editor: Pablo Martín-Ramos

Received: 12 May 2026
Revised: 23 June 2026
Accepted: 24 June 2026
Published: 25 June 2026

Copyright: © 2026 by the authors. Licensee MDPI, Basel, Switzerland. This article is an open access article distributed under the terms and conditions of the Creative Commons Attribution (CC BY) license.

1. Introduction

Soil infiltration in karst landforms is a complex hydrological process jointly controlled by soil, vegetation, climate, and the rock–soil interface [1–3]. Compared with common landforms, the soil infiltration process in karst areas is more complex and variable, which us mainly attributed to the unique geological structure and surface cover characteristics

of these regions [4]. As a key geomorphic element of karst, mountainous terrain not only shapes the soil structure, composition, and properties, but also dominates the non-uniformity and rapidity of infiltration through the unique double-layer structure formed by the surface soil and the underlying bedrock, becoming the core controlling factor of the karst soil infiltration process [5–7].

Surface soil heterogeneity in karst mountainous terrain creates favorable spatial conditions for preferential flow, a key hydrological link between soil water infiltration and surface runoff [8–11]. First, as the core geological interface of karst landforms, the rock–soil interface regulates infiltration through its unique structure and permeability, serving both as a rapid water channel and as a modifier of soil properties via its physicochemical characteristics [12–14]. Second, during ecological succession, plants improve soil hydrology through root growth and litter accumulation, which increase organic matter, optimize pore structure, and enhance permeability and water retention, thereby promoting preferential flow development [15–17]. However, this positive effect reduces the relative importance of the rock–soil interface as a rapid infiltration pathway, leading to a reduction in its contribution to soil infiltration and hydrological recharge [18,19]. This dynamic change reveals the complexity and spatiotemporal variability of the soil infiltration process in karst landforms. Currently, systematic research on the infiltration of different soil layers on slopes, the spatial pattern of soil water, and multi-scale hydrological processes is still lacking.

In a karst slope ecosystem, the spatial heterogeneity of soil water infiltration is mainly influenced by the effects of topography, soil physical properties, and vegetation coverage patterns [20–22]. The heterogeneity of karst fissures and soil structure provides the basis for this, while the diverse soil types and complex vertical soil layer structures further intensify spatial differentiation [23–25]. For instance, in areas where karst fissures are well developed, the hydraulic resistance gradient at the interface between soil and bedrock during heavy rainfall will drive underground lateral flow, resulting in significant differences in infiltration rates at different slopes and obvious variations in vertical infiltration depth [26,27]. Meanwhile, topography indirectly affects infiltration capacity by regulating vegetation distribution and soil erosion processes [28,29]. In steep-slope areas, heavy rain causes surface runoff to flow down the slope and promotes the coupling of lateral flow and preferential flow. A flat plot shows a "low runoff—high infiltration" pattern, and the infiltration process is more dependent on the soil's own water-holding and water-conducting properties [30–32]. Soil physical properties are the intrinsic controlling factors of the infiltration process, and indicators such as bulk density, pore structure, and organic matter content jointly constitute its regulatory network [33,34]. In addition, the karst binary structure forms a unique infiltration interface, which is more likely to trigger preferential flow under higher rainfall intensity [35–37]. While previous studies have identified these individual controlling factors, a key knowledge gap remains: it is unclear whether the observed spatial variation in infiltration patterns is driven more by topographic position per se or by the correlated changes in soil physical properties along the slope.

This study took an abandoned farmland on a karst slope as its object, with two objectives: to characterize the spatiotemporal variations in soil moisture at different slope positions and soil depths through one year of continuous field monitoring, and to identify the dominant water infiltration pathways and their spatial distribution along the topographic gradient using dye tracer experiments and subsequent soil property analysis. We aimed to elucidate how topography regulates the coupled dynamics of soil moisture storage and infiltration behavior in karst slope ecosystems. It should be noted that, since all observations were made along a single slope, the effects of topographic position and associated changes in soil properties cannot be fully separated in this study. It is expected

that the findings will provide theoretical guidance for the protection, management, and sustainable utilization of this type of ecosystem.

2. Materials and Methods

2.1. Study Site Description

The study area was located in Lvhua Township, Qianxi City, Guizhou Province (26°57′00″ N, 106°6′36″ E, 1285~1340 m a.s.l.) (Figure 1a). It has a subtropical monsoon climate, with a stable average annual temperature of 13.8 °C and annual rainfall of 1000–1500 mm. During the one-year observation period, total rainfall reached 1286 mm, with 82% occurring from May to October. Antecedent moisture conditions varied across seasons. The soil was relatively dry (mean $\theta \approx 0.18$ cm^3/cm^3) before the rainy season onset, wet (mean $\theta \approx 0.32$ cm^3/cm^3) during the peak rainy months, and moderately moist during the transition periods. Rainfall intensity was classified as light (<10 mm/h) for 62% of rainy days, moderate (10–25 mm/h) for 24%, and heavy (> 25 mm/h) for 14%. The regional karst landform was developed in Permian carbonate rocks, with high-purity limestone as the main bedrock. It has a high degree of weathering and is mostly covered by soil and vegetation.

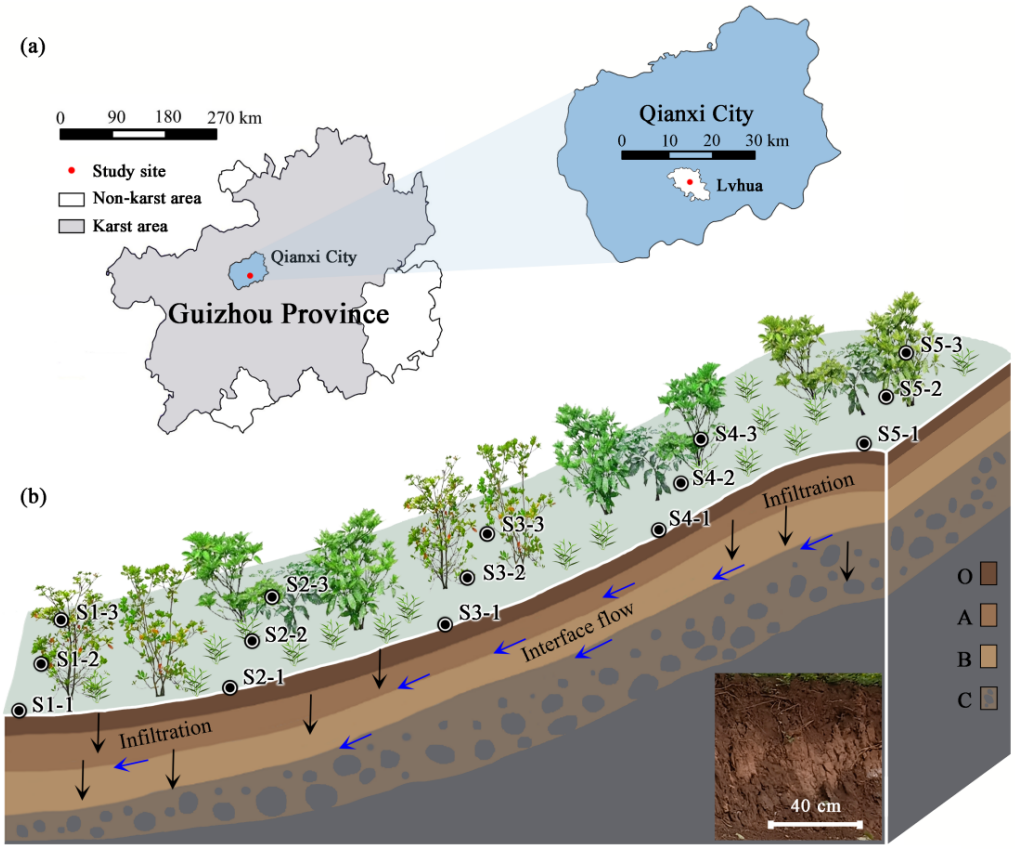


Figure 1. Schematic diagrams of the study plot. (**a**) Geographical location of the plot; (**b**) soil moisture measurement points at different slope positions of the investigated hillside.

The farmland selected for the study was located on the gentle slope of a karst hillside (Figure 1b). The slope faced south and was 165 m long. The soil layer thickness was greater than 40 cm. The soil type was mainly calcareous soil, and the texture was loam clay to clay. The vegetation in this plot was mainly composed of suffruticosa plants such as *Myrsine africana* L., *Rosa roxburghii* Tratt. and *Pyracantha fortuneana* (Maxim.) Li, accompanied by wild grasses such as *Imperata cylindrica* (L.) Beauv. and *Bidens pilosa* L. This abandoned farmland has not been cultivated for many years. The terrain was mainly

composed of micro-habitats formed of rock outcrops, with a high content of rock fragments and strong permeability. Water loss is the main environmental problem in this area, with the main cause being the shallow soil layer. High soil infiltration rate and highly weathered rock lead to intense underground rainstorm flows after heavy rainfall, which has become the main mechanism of soil erosion, as well as soil water loss on the sloping farmland, in this karst area.

2.2. Data and Methods

2.2.1. Soil Moisture Measurement

Based on the characteristics of terrain gradient changes, the slopes in the study area were divided into five gradient zones from S1 to S5, from the foot to the top of the hillslope (Figure 1). The slope angle of each gradient zone were measured on-site using a geological compass (DQL-8, Harbin Optical Instrument Factory Co., Ltd., Harbin, China), with the measured range being 17° to 27°. To construct a control system, five sampling points were randomly set up in the flat plot (slope 0°) far from the hillside to compare and analyze the differences in soil moisture content distribution between the slope gradient zone and the flat environment.

Soil moisture was measured in situ using a portable moisture meter (PR2/4, Delta-T Devices Ltd., Cambridge, UK) at depths of 10, 20, 30, and 40 cm. Measurements were taken monthly from January to December 2025 along the topographic gradient at slope positions S1–S5 and on a flat control plot. Each measurement campaign was completed within a single day. There was no precipitation during the measurement process either, and no extreme rainfall events during the observation period that could significantly affect soil moisture dynamics.

2.2.2. Measurement of Environmental Factors and Soil Conditions

This study determined the key environmental factors at each measurement point, including altitude, slope, soil thickness, rock fragment content, canopy density, and root biomass. Soil sampling and environmental factor measurement were carried out simultaneously. The soil property characteristics at sites S1–S5 were measured by excavating the soil profile. Soil samples at depths of 0–40 cm were obtained using the undisturbed soil sampling method. At the four stratified depths of 10 cm, 20 cm, 30 cm, and 40 cm, three independent and repeated samples were collected from each soil layer.

Samples were used for testing the following key physical and chemical properties: soil bulk density (BD), capillary porosity (CP), non-capillary porosity (NCP), total porosity (TP), soil organic matter (SOM), and >2 mm soil macro-aggregate (SMA) content. All assays were conducted in accordance with standard laboratory methods to ensure the scientific nature and comparability of the data. Soil sampling was conducted in July (mid-rainy season) under representative wet conditions, with three replicate plots established at each of the five slope positions (S1–S5), yielding a total of 15 experimental units. The three replicates at each slope position were spatially independent, with a minimum distance of >15 m between them. The same design was applied to the dye tracer experiment.

2.2.3. Dye Tracer Test

This study simulated the soil moisture transport behavior during rainfall through dye irrigation experiments. The method was as follows: Bright blue FCF dye was used to track soil moisture infiltration in five topographic gradient zones (S1–S5) with antecedent soil moisture 18.83% at 0–40 cm depth. The antecedent soil moisture was measured separately at each slope position, and no significant differences were found among the five positions. Three repeated experiments were set for each gradient zone, with a total of 15 square experimental plots each 1 m^2 in size. At each staining site, a stainless steel ring (20.0 cm

in height and 30.0 cm in diameter) was first vertically inserted into the soil to a depth of 10.0 cm, and then 10 L of dye solution with a concentration of 4.0 $g \cdot L^{-1}$ was injected, approximately equivalent to a local heavy rain event. Twenty-four hours later, a soil profile of 70 cm wide and 80 cm deep was vertically cut along the stained area, and high-resolution digital photography was used for recording. Combining the field-measured scale with image processing software, geometric correction and color standardization processing were carried out on the stained profile image. Dyeing area was quantified using Photoshop CS6 + Matlab R2025b (the steps were based on those in references [3,4,6]). By analyzing the dyeing characteristics, the distribution pattern and spatial correlation of the priority paths of water flow in the soil were revealed, providing a visual basis for quantifying the structural characteristics of the preferential flow channels.

In this study, the following key indicators were quantified in the dye irrigation experiment to analyze the soil moisture infiltration characteristics of the karst surface layer:

Dyeing depth (cm): The vertical depth of soil profile dye infiltration reflects the water infiltration capacity driven by the soil matrix.

Dyeing width (cm): The horizontal staining range of the soil profile reflects the characteristics of lateral diffusion.

Dyeing area (cm^2): The total area of the dye penetration zone in the profile comprehensively reflects the two-dimensional spatial distribution of water transport.

Preferential flow index (%): This reflects the proportion of water transport occurring through macropores and root channels rather than the soil matrix, indicating the efficiency of rapid vertical infiltration. The higher the value, the more significant the phenomenon of preferential flow. The calculation formula is:

$$PFI = \left(1 - \frac{D \times W}{S}\right) \times 100\% \quad (1)$$

where PFI is the preferential flow index (%); D is the uniform infiltration depth (cm), which is the depth at which the staining coverage rate was not less than 80%, indicating the depth at which matrix flow was generally present; W is the width of the soil profile (cm), and S is the total staining area of the soil profile (cm^2).

Lateral flow index (%): This quantifies the extent of horizontal water redistribution, which is critical for understanding downslope water supply and subsurface stormflow generation in hillslope hydrology. The calculation formula is:

$$LFI = \frac{S_{outside}}{S} \times 100\% \quad (2)$$

where the LFI is the lateral flow index (%), Soutside is the dyeing area outside directly beneath the stainless steel ring (cm^2), and S is the total stained area of the soil profile (cm^2).

2.3. Data Analysis

Repeated measures ANOVA was used to evaluate the effects of slope position on soil moisture content, with sampling month as the within-subject factor. One-way ANOVA followed by the least significant difference (LSD) test ($p < 0.05$) was used to compare soil properties and dyeing characteristics among different slope positions. Before analysis, all data were tested for normality and homogeneity of variance. Pearson correlation coefficients (two-tailed) were calculated to assess relationships between soil moisture content and soil properties. All the statistical analyses and data plotting mentioned above were conducted using IBM SPSS Statistics 25 (IBM Corp., Armonk, NY, USA) and Origin 2025 (OriginLab Corp., Northampton, MA, USA).

3. Results

3.1. Soil Water Content

The soil moisture content in the study area increased with depth. The values at 10, 20, 30, and 40 cm were 14.06 ± 0.23%, 15.64 ± 0.28%, 16.89 ± 0.30%, and 18.37 ± 0.32%, respectively. With each 10 cm increase in depth, the mean observed value increased by an average of 1.44%. In terms of temporal dynamics, all depths exhibited a unimodal seasonal pattern, characterized by an inverted U shape (Figure 2). The average moisture content in summer (June to August) was 47% to 65% higher than that in winter (December to February).

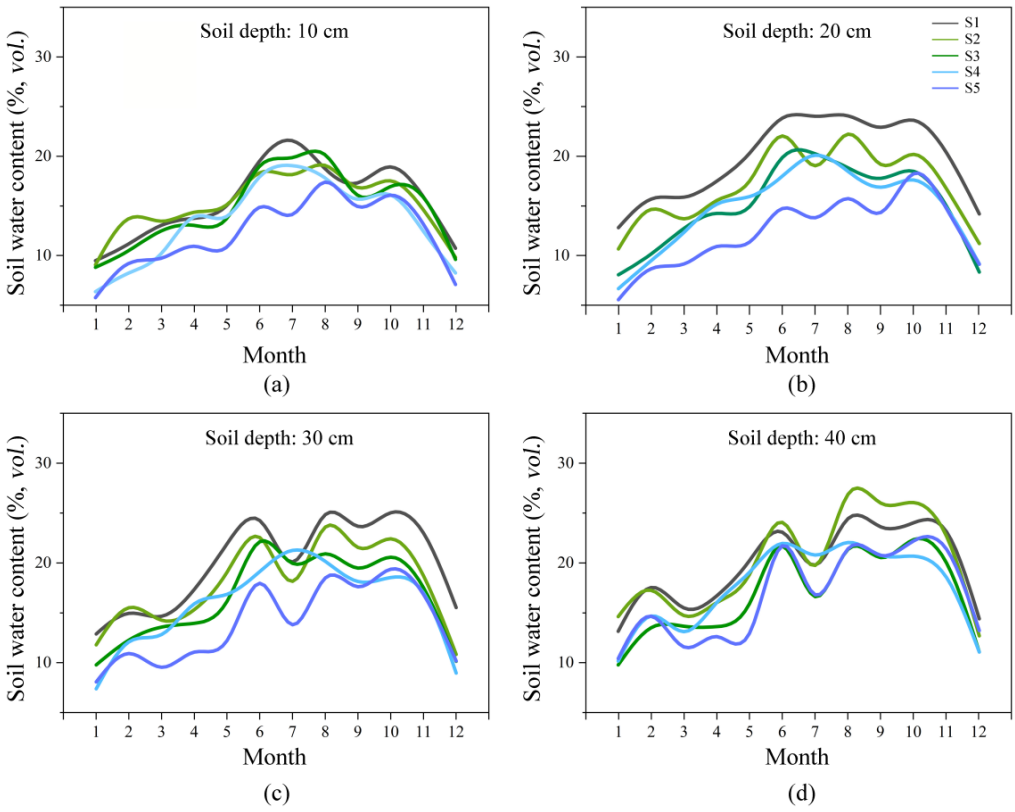


Figure 2. Monthly dynamic changes in soil moisture content at different slope positions and soil depths on the investigated hillslope. (**a**–**d**) The soil moisture content at soil depths of 10, 20, 30, and 40 cm, respectively.

ANOVA showed that the effect of sampling position on soil moisture content was extremely significant, especially during the rainy season (Figure 3). The soil moisture content at the downhill slope positions (S1–S2) was significantly higher than that at the uphill slope positions (S3–S5) ($p < 0.05$). S5 had the lowest value, being 27.4% lower on average annually than S1. S2, S3, and S4 were at intermediate levels, and no significant difference in soil moisture content was observed among certain soil layers at these positions ($p > 0.05$). The soil moisture of the deep layer at S1 was significantly increased, with the value at 40 cm being 27.3% higher than that at 10 cm, indicating that the local environment exerted a regulatory effect on the vertical movement of water.

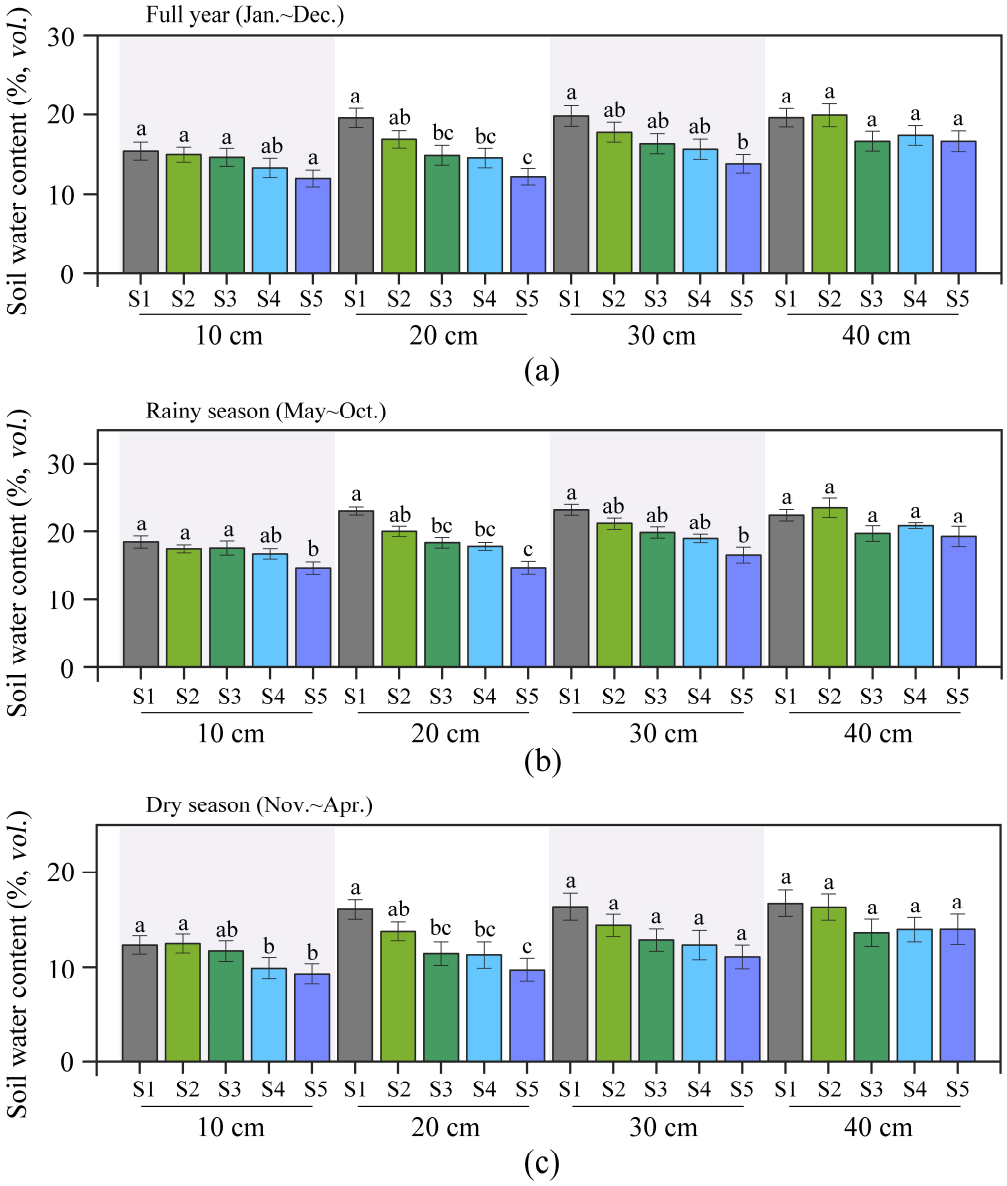


Figure 3. Comparison of annual, rainy season and dry season differences in soil moisture content at different slope positions and soil layer depths. (**a**–**c**) The differences in soil moisture content during the whole year, the rainy season, and the dry season, respectively. Different lowercase letters indicated significant differences ($p < 0.05$) within the same soil depth among different positions.

3.2. Soil Water Content Difference (Δθ)

The Δθ values of different soil layers all gradually decreased with increasing slope height (Figure 4a). Overall, the Δθ of S1 was the highest (+2.51%), while that of S5 was the lowest (−2.45%), resulting in a difference of 4.96%. The Δθ values of S4 and S5 remained in the negative range throughout the year. The values of S2, S3, and S4 were at an intermediate level, and no significant differences were shown among them ($p > 0.05$). It is worth noting that at a depth of 40 cm, the Δθ value of S3 had dropped sharply. The ridge map further reveals the complex distribution pattern of Δθ in soil depth and terrain position (Figure 4b). At a given slope position, deeper soil Δθ generally displayed greater variability compared to shallower soil. Overall, the Δθ of S1, S2, and S5 increased with depth, whereas for S3, S4, and S5, Δθ decreased as depth increased.

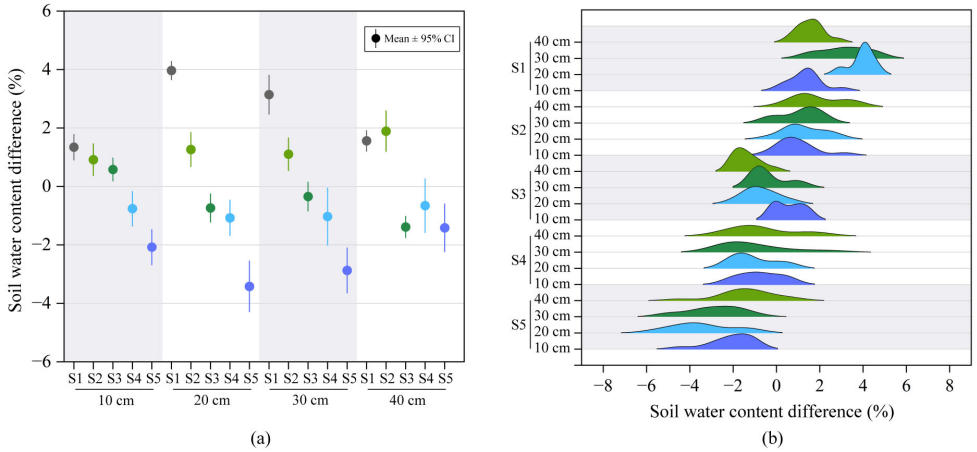


Figure 4. The variation in the difference in soil moisture content between the investigated hillslope and flat plot at different slope positions and soil depths. (**a**) Comparison of soil moisture at the same soil depth across different slope positions; (**b**) comparison of soil moisture at different soil depths for the same slope position.

3.3. Dyeing Characteristics

The dyeing characteristics of the five soil profiles were significantly different (S1–S5; Figure 5, $p < 0.05$). The dyeing depth decreased from 57.3 ± 1.5 cm at S1 to 43.1 ± 1.1 cm at S5, a reduction of 24.8%. However, the dyeing width increased from 42.8 cm for S1 to 53.8 ± 1.6 cm for S4, and then slightly decreased to 51.7 ± 1.6 cm for S5. Therefore, the total dyed area decreased by 30.2%, from 1.49 × 10^3 cm^2 for S1 to 1.04 × 10^3 cm^2 for S5. From S1 to S5, the preferential flow ratio decreased with the increase in the slope position, dropping from 46.6 ± 2.3% for S1 to 34.7 ± 2.1% for S5, with a difference of approximately 12%. The lateral flow index first increased and then decreased, reaching a peak of 21.4 ± 2.7% at S3 and a minimum of 10.9 ± 0.8% at S1. Overall, the infiltration pattern changed from a deep narrow preferential channel (S1) to a shallow wide diffusion seepage pattern (S5).

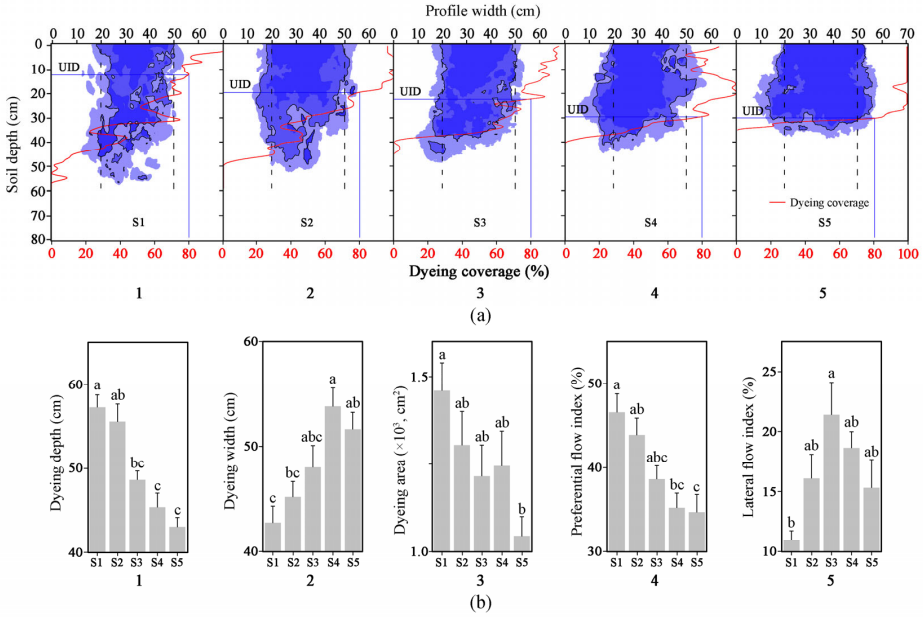


Figure 5. The characteristics of the stained tracer profile at different positions along the investigated hillslope. (**a**) Dye tracer infiltration pattern; (**b**) comparison of differences in dyeing characteristics. Different lowercase letters indicated significant differences ($p < 0.05$) among different positions. UID was the uniform infiltration depth where the dyeing coverage equaled 80%, indicating the depth of the matrix flow.

3.4. Relationship Between Soil Properties and Soil Moisture Content/Dyeing Characteristics

The environmental characteristics of the studied sloping farmland are shown in Table 1, and the basic physical and chemical properties of the soil at each monitoring point are detailed in Table 2. There was a significant correlation among soil property indicators (Figure 6). Pearson correlation analysis showed that BD was extremely significantly negatively correlated with CP, NCP, TP, SOM and SMA. There was a significant positive correlation among CP, NCP and TP, as well as between these three porosity parameters and SOM and SMA. Soil moisture content showed a high correlation with the above indicators, with an extremely significant negative correlation with BD and an extremely significant positive correlation with CP, NCP, TP, SOM and SMA.

Table 1. Environmental characteristics of different slope positions on the study hillslope.

Position	Altitude (m)	Slope (°)	Soil Thickness (cm)	Rock Fragment Content (%)	Vegetation Coverage (%)	Root Biomass (kg/m^2)
S1	1291.67 ± 2.33 e	17.50 ± 0.15 d	135.93 ± 5.97 a	15.07 ± 1.53 c	71.33 ± 1.24 a	2.21 ± 0.08 a
S2	1305.33 ± 1.20 d	19.73 ± 0.19 cd	103.37 ± 5.94 b	16.77 ± 1.25 bc	68.13 ± 1.83 ab	2.01 ± 0.04 ab
S3	1315.00 ± 0.58 c	26.77 ± 1.17 a	76.07 ± 4.75 c	21.53 ± 1.33 ab	64.63 ± 2.20 abc	1.75 ± 0.05 bc
S4	1326.67 ± 1.45 b	24.73 ± 0.79 ab	64.53 ± 2.35 cd	20.83 ± 1.13 ab	60.23 ± 1.99 bc	1.54 ± 0.10 c
S5	1339.33 ± 1.20 a	22.17 ± 1.06 bc	51.07 ± 2.92 d	22.47 ± 0.69 a	59.00 ± 1.91 c	1.45 ± 0.05 c

The values in the above table are the mean ± standard error. Different lowercase letters indicated significant differences ($p < 0.05$) among different positions.

Table 2. Soil properties at different slope positions and soil depths on the investigated hillslope.

Soil Depth (cm)	Position	BD (g/cm^3)	CP (%)	NCP (%)	TP (%)	SOM (g/kg)	SMA(%)
10	S1	1.16 ± 0.01 b	48.47 ± 0.68 a	8.47 ± 0.43 a	56.94 ± 1.11 a	53.62 ± 1.26 a	51.93 ± 2.59 a
	S2	1.16 ± 0.03 ab	48.89 ± 0.25 a	7.65 ± 0.44 ab	56.54 ± 0.68 a	51.09 ± 2.29 ab	46.88 ± 1.24 a
	S3	1.19 ± 0.02 ab	48.11 ± 0.54 a	6.76 ± 0.41 abc	54.87 ± 0.95 a	43.32 ± 2.18 bc	36.99 ± 0.95 b
	S4	1.21 ± 0.02 ab	48.61 ± 0.86 a	5.86 ± 0.39 bc	54.47 ± 1.25 a	43.02 ± 1.48 c	34.83 ± 1.62 b
	S5	1.24 ± 0.01 a	48.56 ± 0.70 a	4.96 ± 0.41 c	53.53 ± 1.08 a	41.73 ± 0.65 c	38.29 ± 1.40 b
20	S1	1.19 ± 0.01 c	47.06 ± 1.09 a	8.14 ± 0.36 a	55.20 ± 1.44 a	43.64 ± 1.52 a	38.25 ± 2.07 ab
	S2	1.25 ± 0.03 bc	44.68 ± 0.15 ab	7.22 ± 0.38 ab	51.90 ± 0.53 ab	44.73 ± 2.22 a	41.91 ± 1.94 a
	S3	1.29 ± 0.01 ab	45.02 ± 0.79 ab	6.48 ± 0.38 abc	51.50 ± 1.13 ab	35.55 ± 1.53 b	27.12 ± 0.88 c
	S4	1.31 ± 0.01 ab	43.84 ± 0.28 b	5.55 ± 0.44 bc	49.39 ± 0.72 b	34.69 ± 1.58 b	31.80 ± 1.46 bc
	S5	1.35 ± 0.01 a	43.75 ± 0.45 b	4.62 ± 0.57 c	48.36 ± 1.02 b	34.24 ± 0.87 b	30.68 ± 0.91 c
30	S1	1.24 ± 0.03 c	45.85 ± 0.92 a	7.27 ± 0.40 a	53.12 ± 1.27 ab	41.72 ± 0.82 a	35.40 ± 2.44 a
	S2	1.28 ± 0.02 bc	45.36 ± 0.95 a	7.81 ± 0.61 a	53.17 ± 0.37 a	37.28 ± 1.46 ab	33.16 ± 2.80 a
	S3	1.31 ± 0.01 bc	43.25 ± 0.18 ab	6.20 ± 0.66 ab	49.45 ± 0.56 abc	35.60 ± 1.09 b	31.89 ± 0.30 a
	S4	1.35 ± 0.01 ab	43.64 ± 0.31 ab	5.65 ± 0.62 ab	49.26 ± 0.86 bc	28.41 ± 1.08 c	20.69 ± 0.73 b
	S5	1.39 ± 0.02 a	42.18 ± 0.36 b	4.51 ± 0.49 b	46.68 ± 0.85 c	27.57 ± 0.77 c	19.82 ± 0.83 b
40	S1	1.31 ± 0.03 c	42.74 ± 1.69 a	7.97 ± 0.34 a	50.71 ± 2.03 a	34.98 ± 0.89 a	30.78 ± 1.60 a
	S2	1.34 ± 0.01 c	43.08 ± 0.63 a	7.12 ± 0.37 a	50.20 ± 1.00 ab	28.85 ± 1.92 b	26.61 ± 1.50 ab
	S3	1.38 ± 0.01 bc	42.34 ± 0.68 a	6.18 ± 0.33 ab	48.52 ± 0.99 ab	28.30 ± 1.13 b	21.12 ± 0.98 bc
	S4	1.42 ± 0.01 ab	42.24 ± 0.30 a	5.09 ± 0.51 bc	47.34 ± 0.81 ab	28.72 ± 0.54 b	25.09 ± 1.37 ab
	S5	1.46 ± 0.02 a	40.74 ± 0.41 a	4.18 ± 0.40 c	44.92 ± 0.80 b	25.27 ± 0.78 b	16.28 ± 1.64 c

The values in the above table are the mean ± standard error. Different lowercase letters indicated significant differences ($p < 0.05$) within the same soil depth among different positions. BD, bulk density; CP, capillary porosity; NCP, non-capillary porosity; TP, total porosity; SOM, soil organic matter content; SMA, soil macro-aggregate content.

There was also a significant correlation between soil property indicators and dyeing characteristic indicators (Table 3). BD was extremely significantly negatively correlated with the dyeing depth, dyeing area, and preferential flow index, while CP, NCP, TP, SOM and SMA were extremely significantly positively correlated with these three indicators. Dyeing width was positively correlated with BD and significantly negatively correlated with the CP, NCP, TP, SOM, and SMA. However, no significant correlation was found between the lateral flow index and the measured soil properties, suggesting that it might be more influenced by topographic factors.

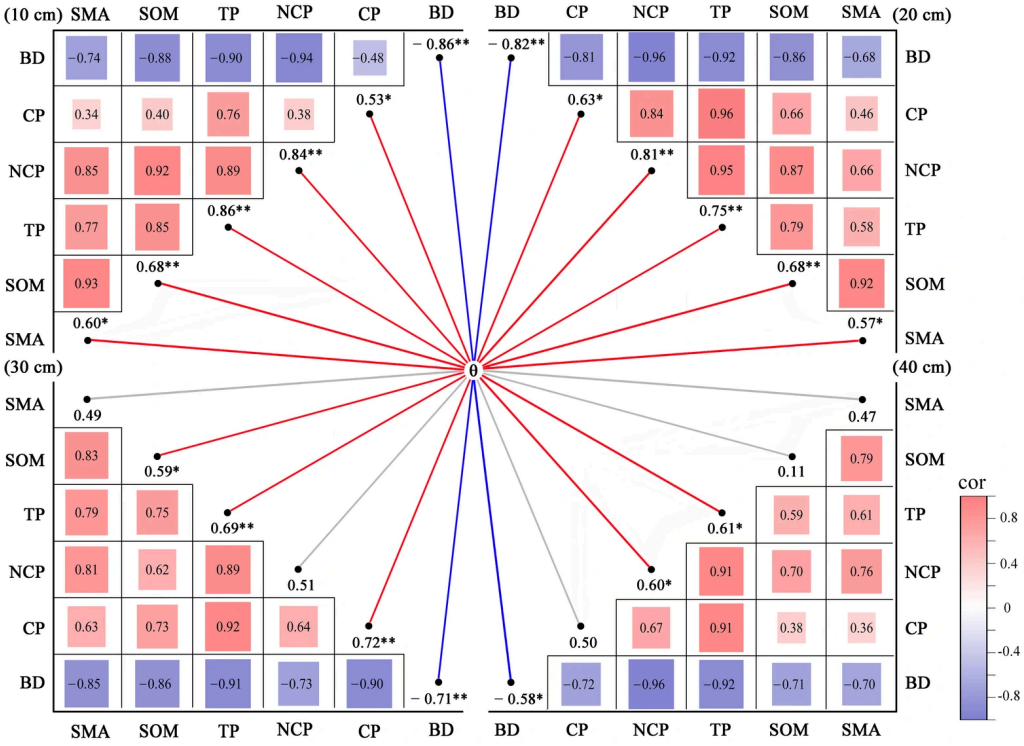


Figure 6. Heat maps of the correlation between soil moisture content (θ) at different depths and key soil physical properties. BD, bulk density; CP, capillary porosity; NCP, non-capillary porosity; TP, total porosity; SOM, soil organic matter content; SMA, soil macro-aggregate content. *, $p < 0.05$, **, $p < 0.01$.

Table 3. Correlation coefficients between dyeing characteristics and soil properties.

Soil Property (0–40 cm)	Dyeing Depth (cm)	Dyeing Width (cm)	Dyeing Area (cm^2)	Preferential Flow Index (%)	Lateral Flow Index (%)
Bulk density	−0.89 **	0.63 *	−0.77 **	−0.75 **	0.32
Capillary porosity	0.69 **	−0.41	0.66 **	0.58 *	−0.32
Non-capillary porosity	0.90 **	−0.62 *	0.75 **	0.70 **	−0.24
Total porosity	0.84 **	−0.55 *	0.74 **	0.67 **	−0.28
Soil organic matter content	0.92 **	−0.68 **	0.79 **	0.78 **	−0.42
Soil macro-aggregate content	0.90 **	−0.73 **	0.65 **	0.80 **	−0.47

* indicates a significant correlation ($p < 0.05$), ** indicates an extremely significant correlation ($p < 0.01$).

4. Discussion

4.1. The Variation Characteristics of Soil Moisture Content Distribution Along the Slope

The soil moisture on karst slopes has obvious vertical differentiation characteristics. The annual average observed value increased from 14.06% at 10 cm to 18.37% at 40 cm with an increase in depth. This vertical increase trend is consistent with the previous research results in karst areas [38–40], partly due to the water-blocking effect of the bedrock, which often hinders further vertical infiltration [41–43]. The moisture content of deep soil shows an inverted U-shaped seasonal variation, with summer being 47% to 65% higher than winter, reflecting the typical seasonal rainfall pattern of the subtropical monsoon climate.

There were also significant differences in soil moisture along the slope. The soil moisture at the downhill position (S1–S2) was significantly higher than that at the uphill position (S3–S5), among which the annual average value of S5 was the lowest, 27.4% lower than that of S1. This pattern is consistent with the previous reports that the moisture content on the uphill slope is 45.3–69.8% of that on the downhill slope [44–46]. However, the magnitude of the difference observed in this study (27.4% reduction) falls at the lower end of this reported range, suggesting a relatively stronger slope effect at our site. The

downhill section can accept the runoff from the uphill section and lateral replenishment, and the water conditions are relatively good. However, the terrain of the uphill section is higher, and water is prone to loss. The interaction between slope position and soil depth was significant, with the most abundant content at S1 (the moisture content at 40 cm was 27.3% higher than that at 10 cm), indicating that local conditions affect vertical moisture redistribution. Possible influencing factors include differences in soil thickness, organic matter content and root distribution along the slope, although the relative importance of each factor cannot be separated from the current data. This depth-related pattern is consistent with findings from other karst studies, although the degree of deep-layer enrichment at S1 was more pronounced than typically reported.

This study examined the difference in soil moisture ($\Delta\theta$) between the slope position and the flat control plot. The slope of $\Delta\theta$ shows a downward trend from the bottom (S1: +2.51%) to the top (S5: −2.45%), with S4 and S5 being negative throughout the year. This spatial pattern indicates that, compared with the flat plot, the moisture content at the uphill position is lower, while that at the downhill position is higher. This spatial pattern of $\Delta\theta$ decreasing with slope height is consistent with previous karst studies [47–49]. Several factors were related to this pattern, including soil thickness, organic matter content, vegetation coverage and rock debris content along the slope, as well as potential water redistribution on the downhill slope. In addition, due to the relatively shallow soil layer on the karst slope and its poor water-holding capacity, coupled with soil erosion along the slope, the rock and soil structure and water process from bottom to top show obvious heterogeneity.

The vertical distribution of $\Delta\theta$ varies with different slope positions. At S1, S2 and S5, $\Delta\theta$ increases with depth, while at S3 and S4, it decreases with depth. This contrasts with studies from karst trough valleys where $\Delta\theta$ consistently decreased with depth, suggesting that local topographic and soil conditions may modulate the vertical pattern of water redistribution. The reasons for this different pattern cannot be determined solely from the current data, but it may reflect the differences in local soil properties and drainage conditions. It is notable that there was a sharp decrease in $\Delta\theta$ at the S3 40 cm layer, although the underlying mechanism requires further study through additional measurements. Overall, the $\Delta\theta$ pattern observed in this study provides descriptive characteristics of the spatial variation in soil moisture along the slope, rather than direct evidence of a specific hydrological process.

4.2. The Variation Characteristics of Soil Moisture Infiltration Along the Slope

Observations along the slope from the downhill position (S1) to the uphill position (S5) showed that the dyeing depth decreased from 57.3 cm to 43.1 cm, with a reduction rate of 24.8%. The dyeing width increased from 42.8 cm for S1 to 53.8 cm for S4 (slightly decreased to 51.7 cm for S5). This pattern is consistent with observations from karst peak-cluster depression studies [50,51], suggesting a gradual shift from deeper, narrower vertical infiltration at downhill positions to shallower, wider lateral spreading at uphill positions. This phenomenon may be related to the spatial heterogeneity of the soil-surface karst zone structure on the karst slope. The soil at downhill positions was thicker, and the surface karst zone exhibited greater fissure development, which may facilitate rapid infiltration along preferred pathways. At uphill positions, the shallower soil and proximity to bedrock may promote lateral water diffusion at the soil–rock interface. For instance, observations at the Huanjiang Karst Station show that the migration speed of the wet front gradually slows down from the downhill area to the uphill area. Moreover, the infiltration in the thick-soil area was less affected by the hydraulic gradient, while the infiltration in the shallow-soil area varies greatly, confirming the regulatory effect of the terrain on the vertical

distribution of water [52,53]. These observations suggest that topographic conditions are associated with variations in infiltration patterns along karst slopes, potentially through their influence on soil thickness and subsurface structure (Figure 7). It should be noted that Figure 7 presents a conceptual framework based on the current dataset, which requires further validation with additional measurements.

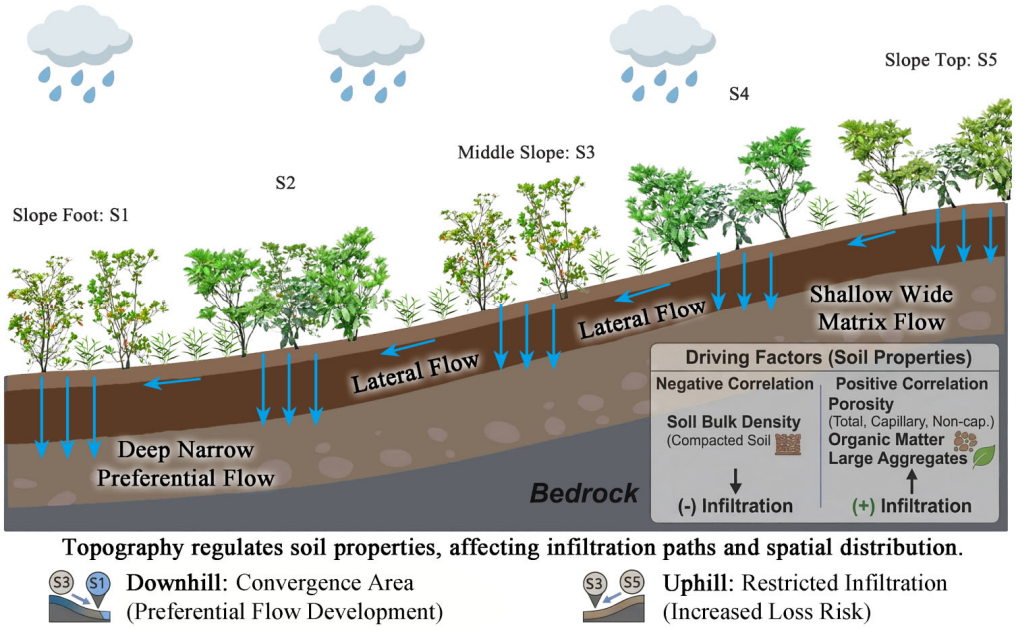


Figure 7. Conceptual map of the main water infiltration patterns integrating different slope positions and soil properties on karst hillslope.

The transformation of the infiltration path was further reflected in the slope position difference in the water transport pattern. The proportion of preferential flow decreased from 46.6% at S1 to 34.7% at S5, a pattern consistent with observations from other karst peak area studies [54–56]. The greater decrease observed in this study (24.8%) may be associated with the steeper slope gradient at our site, although direct measurements of fissure density are not available to confirm this relationship. The peak lateral flow at S3 (21.4%) may reflect local variations in slope geometry or subsurface conditions, although the specific mechanisms cannot be determined from the current dataset. This slope pattern of water distribution appears to differ from patterns typically reported in non-karst areas [30,32], possibly reflecting the influence of bedrock exposure and heterogeneous subsurface structure characteristic of karst landscapes. The latter usually shows a homogeneous infiltration feature where the infiltration volume decreases linearly with the increase in slope. However, in karst areas, due to the high exposure rate of bedrock and the oblique distribution of rocks in the form of boulders, the infiltration increment can be significantly affected, intensifying the heterogeneity of the infiltration path.

The infiltration distribution pattern observed along the slope may be associated with spatial differences in eco-hydrological conditions, although direct measurements of ecological functions were not included in this study. In this study, the total dyed area decreased from 1.49×10^3 cm^2 at S1 to 1.04×10^3 cm^2 at S5, a reduction of 30.2%, which was directly related to the slope position difference in vegetation water availability. The deeper soil and more developed preferential flow system at downhill positions (high pore flow >63%) suggest greater water availability at these locations, which may benefit vegetation growth. At uphill positions, the shallower soil and lower water storage capacity may subject vegetation to greater drought stress, although plant physiological measurements are needed to confirm this inference. Previous studies [57,58] have suggested that vegetation in karst

landscapes may exhibit adaptive responses to such spatial differences in water availability, with plants at downhill positions benefiting from deeper preferential flow and plants at uphill positions potentially adopting drought-coping strategies. Direct measurements of plant water use were beyond the scope of this study.

4.3. The Influence of Soil Conditions on Soil Moisture and Infiltration Patterns

This study demonstrated that BD was significantly and negatively correlated with dyeing depth, dyeing area, and preferential flow index. CP, TP, SOM, and SMA were significantly and positively correlated with the above three indicators. This association suggests that soil layers with higher organic matter, porosity, and aggregate content tend to exhibit greater permeability and water storage potential, which is consistent with the known effects of these properties on capillary water-holding capacity and bulk density. Conversely, compacted layers tended to show lower water content, likely associated with reduced pore space and lower hydraulic conductivity. The contents of CP, SOM, and SMA were significantly higher at downhill positions compared to uphill positions, and these differences were associated with greater macro-pore flow development at downhill sites. However, on the uphill slope, due to the weakening of soil accumulation, the preferential flow path was blocked, and the proportion of lateral flow at the rock–soil interface increased. The observational results of other studies confirm this rule: the wet front velocity on slopes covered with shallow soil is much higher than that in non-karst areas, and the slope position difference is significant—the wet front velocity increases from the uphill area to the downhill area, and the proportion of preferential flow is higher in the downhill area [10,44,53]. The negative effect of slope on soil layer thickness was particularly prominent, resulting in the thinning of the organic matter layer, which echoes the negative correlation of BD-SOM.

Soil moisture was found to be positively associated with CP, TP, SOM, and SMA. This association is consistent with the known role of organic matter in facilitating micro-aggregate formation into macro-aggregates, which tends to increase pore volume and enhance soil moisture retention. However, the proportion of lateral flow showed no significant correlation with soil properties, suggesting that it may be more influenced by local factors such as micro-topography, soil–rock interfaces, or transient hydraulic gradients [7,20,38]. For instance, the lateral flow in the middle of the slope (S3 point) was significantly higher than that in the upper and lower parts of the slope, which was consistent with the characteristic of terrain slope as a proxy indicator of hydraulic gradient—steep slopes have poor water retention capacity. Some of the infiltration water flowed down the slope, while vertical infiltration was stronger in the low-slope area. The hydrological processes at different slopes vary significantly: At the downhill slope, the combination of thicker soil, higher porosity, and greater SOM/SMA content was associated with more developed vertical preferential flow channels and higher post-rainfall water storage potential; the opposite was true at the uphill slope. Furthermore, plant roots enhance hydraulic conductivity by creating preferential flow channels [4,50,53]. For instance, in the slopes of natural forests, the preferential flow of karst soil is mainly funnel- and branch-shaped, and the underground flow with the strongest lateral expansion occurs within a 30 cm range at the top of the soil profile in areas with well-developed lateral root systems [4,15,55]. In conclusion, the observed infiltration patterns were associated with the combined influence of topography, rainfall, soil conditions, and root systems, suggesting a potential control chain involving slope position, soil thickness, and root development.

Several limitations of the dye tracer method should be acknowledged. Firstly, the two-dimensional slice images capture only vertical dye distribution and cannot fully represent the three-dimensional architecture of preferential flow networks. Secondly, the experiment

was conducted under a single antecedent moisture condition (18.83%), whereas infiltration pathways can shift significantly under drier or wetter initial states. Thirdly, the results are scale-dependent, as the small plot size may not capture larger-scale macropore connectivity. Finally, the single-time-point measurement cannot reflect temporal variability in flow path activation across different rainfall events and seasons.

5. Conclusions

Based on a one-year in situ monitoring and dye tracer experiment on abandoned farmland on a single karst slope, the spatial differentiation laws and driving mechanisms of hydrological processes were revealed. The research results show that soil moisture exhibits obvious vertical and slope differentiation. The distribution of $\Delta\theta$ confirms the water transport process along the slope after rainfall. The uphill sections (S4 and S5) were the water conveyance areas, while the downhill sections (S1 and S2) were the enrichment areas. The infiltration path varied with an increase in slope position. At the downhill position, the deep vertical preferential flow was dominant and the PFI was relatively high. At the uphill position, it turned into a shallow lateral diffuse flow, and the LFI reached its peak (S3) in the middle of the slope. Soil physical properties were key regulatory factors. BD was negatively correlated with the infiltration volume, while CP, NCP, TP, SOM, and SMA were positively correlated. In this study, the topographic gradient formed a potential regulation mechanism of topography–soil properties–infiltration path/water distribution by influencing the spatial distribution of soil properties along a single karst slope. The downhill position was more conducive to preferential flow development, acting as a water convergence zone, while the uphill position restricted infiltration and exhibited greater runoff loss risk. These findings provide a scientific basis for understanding hydrological processes and vegetation adaptation strategies on abandoned farmland on karst slopes. Caution is needed when extrapolating to other sites due to the inherent variability in karst landscapes, and the results require verification on additional slopes with different soil, geomorphological and agrotechnical conditions.

Supplementary Materials: The following supporting information can be downloaded at: https://www.mdpi.com/article/10.3390/agronomy16131237/s1, Table S1: Characteristics of environmental factors at different slope positions on the sloping farmland; Table S2: Soil properties at different slope positions and soil layer depths on the sloping farmland; Table S3: Soil moisture content at different slope positions and depths on the sloping farmland; Table S4: The profile characteristics of the staining tracer at different positions along the sloping farmland; Table S5: The soil moisture content of the control group in the flat sample plot.

Author Contributions: Conceptualization, Z.Z. and J.Z.; methodology, Z.Z.; software, Z.Z. and J.Z.; validation, Z.Z. and J.Z.; formal analysis, Z.Z.; investigation, Z.Z.; resources, Z.Z.; data curation, Z.Z.; writing—original draft preparation. Z.Z.; writing—review and editing Z.Z.; visualization, Z.Z. and J.Z.; supervision, Z.Z. and J.Z.; project administration, Z.Z.; funding acquisition, Z.Z. All authors have read and agreed to the published version of the manuscript.

Funding: This research was funded by the Guizhou Provincial Basic Research Program (Natural Science) (grant number: QKHJC-MS [2026]479; funder: Department of Science and Technology of Guizhou Province) and Natural Science Research Project of Guizhou Education University (grant number: 2025GCC008; funder: Guizhou Education University).

Data Availability Statement: The original contributions presented in this study are included in the article/Supplementary Material. Further inquiries can be directed to the corresponding author.

Conflicts of Interest: The authors declare no conflicts of interest.

References

1. Liu, J.X.; Deng, Z.M.; Chen, L.D.; Huang, Y.; Peng, X.Y. Quantifying the influence of soil-rock interfaces on water infiltration rate in karst landscapes. *Geoderma* **2025**, *460*, 117432. [CrossRef]
2. Zhang, Z.C.; Chen, X.; Ghadouani, A.; Shi, P. Modelling hydrological processes influenced by soil, rock and vegetation in a small karst basin of southwest China. *Hydrol. Process.* **2011**, *25*, 2456–2470. [CrossRef]
3. Zhao, Z.M.; Zhang, H.; Zhang, J. Impacts of rock-soil interface on soil infiltration and spatio-temporal water distribution during ecosystem succession in karst areas. *Catena* **2025**, *260*, 109474. [CrossRef]
4. Zhao, Z.M.; Shen, Y.X.; Jiang, R.H.; Wang, Q.H. Rock outcrops change infiltrability and water flow behavior in a karst soil. *Vadose Zone J.* **2020**, *19*, e20002. [CrossRef]
5. Gan, F.L.; Shi, H.L.; Gou, J.F.; Zhang, L.X.; Liu, C.H. Effects of bedrock strata dip on soil infiltration capacity under different land use types in a karst trough valley of Southwest China. *Catena* **2023**, *230*, 107253. [CrossRef]
6. Zhao, Z.M.; Zhang, J.; Liu, R. Application of overground rock film mulching (ORFM) technology in karst rocky desertification farmland: Improving soil moisture environment and crop root growth. *Agronomy* **2024**, *14*, 1265. [CrossRef]
7. Zhang, J.; Chen, H.; Fu, Z.; Luo, Z.; Wang, F.; Wang, K. Effect of soil thickness on rainfall infiltration and runoff generation from karst hillslopes during rainstorms. *Eur. J. Soil Sci.* **2022**, *73*, e13288. [CrossRef]
8. Zhai, M.; Zhao, Y.; Wang, K.; Xiang, J.; Wang, Z.; Pan, Y.; Li, S. Effects of contour antislope terracing on preferential soil flow in sloping farmland in the alpine valley area of Southwest China. *Agronomy* **2025**, *15*, 2101. [CrossRef]
9. Wang, F.; Chen, H.S.; Lian, J.J.; Fu, Z.Y.; Nie, Y.P. Preferential flow in different soil architectures of a small karst catchment. *Vadose Zone J.* **2018**, *17*, 180107. [CrossRef]
10. Zhang, J.; Wang, S.; Fu, Z.Y.; Wang, F.; Wang, K.L.; Chen, H.S. Soil thickness influences the control effect of micro-topography on subsurface runoff generation in the karst hillslope critical zone. *Catena* **2024**, *239*, 107957. [CrossRef]
11. Zhao, S.Y.; Jia, Y.W.; Gong, J.G.; Niu, C.W.; Su, H.D.; Gan, Y.D.; Liu, H. Spatial variability of preferential flow and infiltration redistribution along a rocky-mountain hillslope, northern China. *Water* **2020**, *12*, 1102. [CrossRef]
12. Hegedus-Csondor, K.; Sebe, K.; Molnar, Z.; Dezso, J.; Leelssy, S.; Hegedus, A.; Eross, A. Tracing the transition from hypogene to epigene karstification in the Villány Thermal Karst area, Hungary: Linking submicron-scale cave processes with regional groundwater flow system dynamics. *Hydrogeol. J.* **2025**, *33*, 1109–1131. [CrossRef]
13. Li, Y.; Liu, Z.Q.; Liu, G.H.; Xiong, K.N.; Cai, L.L. Dynamic variations in soil moisture in an epikarst fissure in the karst rocky desertification area. *J. Hydrol.* **2020**, *591*, 125587. [CrossRef]
14. Li, Y.Q.; Wang, S.J.; Peng, T.; Zhao, G.Z.; Dai, B. Hydrological characteristics and available water storage of typical karst soil in SW China under different soil–rock structures. *Geoderma* **2023**, *438*, 116633. [CrossRef]
15. Ding, B.; Cai, X.Y.; Wang, Y.; Li, H.J.; Zhao, X.Z.; Xiao, M.; Li, J.F.; Yu, Q.J.; Zhao, Y. Secondary vegetation succession following reforestation intensifies preferential flow by improving soil structure in the Chinese Karst region. *Ecol. Indic.* **2023**, *156*, 111166. [CrossRef]
16. Zhang, Y.H.; Xu, X.L.; Li, Z.W.; Xu, C.H.; Luo, W. Improvements in soil quality with vegetation succession in subtropical China karst. *Sci. Total Environ.* **2021**, *775*, 145876. [CrossRef] [PubMed]
17. Zhu, H.H.; He, X.Y.; Wang, K.L.; Su, Y.R.; Wu, J.S. Interactions of vegetation succession, soil bio-chemical properties and microbial communities in a Karst ecosystem. *Eur. J. Soil Biol.* **2012**, *51*, 1–7. [CrossRef]
18. Zhao, Z.M.; Shen, Y.X. Rain-induced weathering dissolution of limestone and implications for the soil sinking-rock outcrops emergence mechanism at the karst surface: A case study in southwestern China. *Carbonate. Evaporite.* **2022**, *37*, 69. [CrossRef]
19. Zhang, S.Q.; Ma, Q.H.; Qihua, K.; Zhang, K.L.; Zhu, T. Effects of rock outcrops on runoff and erosion from karst slopes under simulated rainfall. *Land Degrad. Dev.* **2024**, *35*, 949–967. [CrossRef]
20. Chen, X.; Zhang, Z.C.; Chen, X.H.; Shi, P. The impact of land use and land cover changes on soil moisture and hydraulic conductivity along the karst hillslopes of southwest China. *Environ. Earth Sci.* **2009**, *59*, 811–820. [CrossRef]
21. Li, Y.; Li, K.P.; Zhou, Q.W.; Zhao, Y.L.; Cai, L.L.; Yang, Z.Y. Spatiotemporal dynamics and similarity in soil moisture in shallow soils on karst slopes. *J. Hydrol.* **2024**, *639*, 131655. [CrossRef]
22. Zhao, Z.M.; Shen, Y.X.; Wang, Q.H.; Jiang, R.H. The temporal stability of soil moisture spatial pattern and its influencing factors in rocky environments. *Catena* **2020**, *187*, 104418. [CrossRef]
23. Huang, X.F.; Zhang, Z.M.; Zhou, Y.C.; Wang, X.F.; Zhang, J.C.; Zhou, X.W. Spatial heterogeneity of soil thickness and factors controlling it in a karst basin. *Eurasian Soil Sci.* **2021**, *54*, 478–486. [CrossRef]
24. Wang, X.F.; Huang, X.F.; Hu, J.W.; Zhang, Z.M. The spatial distribution characteristics of soil organic carbon and its effects on topsoil under different karst landforms. *Int. J. Environ. Res. Public Health* **2020**, *17*, 2889. [CrossRef] [PubMed]
25. Yang, J.; Chen, H.S.; Nie, Y.P.; Wang, K.L. Dynamic variations in profile soil water on karst hillslopes in Southwest China. *Catena* **2019**, *172*, 655–663. [CrossRef]
26. Fang, Q.; Zi, R.Y.; Zhao, L.S.; Fan, C.H.; Fang, F.Y.; Qian, X.H. Effect of bedrock permeability on runoff and soil loss in soil-mantled karst slopes under successive rainfall conditions. *Catena* **2024**, *247*, 108524. [CrossRef]

27. Peng, X.D.; Dai, Q.H.; Li, C.L.; Zhao, L.S. Role of underground fissure flow in near-surface rainfall-runoff process on a rock mantled slope in the karst rocky desertification area. *Eng. Geol.* **2018**, *243*, 10–17. [CrossRef]
28. Shi, H.L.; Gan, F.L.; Jiang, L.S.; Tan, X.H.; Liu, D.H.; Yan, Y.J.; Fan, Y.C.; Pu, J.B. Responses of soil infiltration and erodibility to vegetation succession stages at erosion and deposition sites in karst trough valleys. *Forests* **2024**, *15*, 2167. [CrossRef]
29. Zhong, F.X.; Xu, X.L.; Li, Z.W.; Zeng, X.M.; Yi, R.Z.; Luo, W.; Zhang, Y.H.; Xu, C.H. Relationships between lithology, topography, soil, and vegetation, and their implications for karst vegetation restoration. *Catena* **2022**, *209*, 105831. [CrossRef]
30. Charlier, J.B.; Moussa, R.; David, P.Y.; Desprats, J.F. Quantifying peakflow attenuation/amplification in a karst river using the diffusive wave model with lateral flow. *Hydrol. Process.* **2019**, *33*, 2337–2354. [CrossRef]
31. Peng, T.; Wang, S. Effects of land use, land cover and rainfall regimes on the surface runoff and soil loss on karst slopes in southwest China. *Catena* **2012**, *90*, 53–62. [CrossRef]
32. Fonseca, M.R.S.; Uagoda, R.E.S.; Chaves, H.M.L. Runoff, soil loss, and water balance in a restored Karst area of the Brazilian Savanna. *CATENA* **2023**, *222*, 106878. [CrossRef]
33. Pla, C.; Cuezva, S.; Martinez-Martinez, J.; Fernandez-Cortes, A.; Garcia-Anton, E.; Fusi, N.; Crosta, G.B.; Cuevas-Gonzalez, J.; Cañaveras, J.C.; Sanchez-Moral, S.; et al. Role of soil pore structure in water infiltration and CO2 exchange between the atmosphere and underground air in the vadose zone: A combined laboratory and field approach. *Catena* **2017**, *149*, 402–416. [CrossRef]
34. Wei, H.; Deng, Y.S.; Huang, J.; He, L.; Tang, Q.Y.; Xiao, Y. A quantitative study of the influence of soil organic carbon and pore characteristics on the stability of aggregates of the karst peak-cluster depression area in Southwest China. *J. Soil Sediment.* **2023**, *23*, 312–330. [CrossRef]
35. Chen, X.; Zhang, Z.C.; Soulsby, C.; Cheng, Q.B.; Binley, A.; Jiang, R.; Tao, M. Characterizing the heterogeneity of karst critical zone and its hydrological function: An integrated approach. *Hydrol. Process.* **2018**, *32*, 2932–2946. [CrossRef]
36. Huang, F.Y.; Gao, Y.; Hu, X.N.; Wang, X.G.; Pu, S.Y. Influence of precipitation infiltration recharge on hydrological processes of the karst aquifer system and adjacent river. *J. Hydrol.* **2024**, *639*, 131656. [CrossRef]
37. Zhao, Z.M.; Shen, Y.X.; Shan, Z.J.; Yu, Y.; Zhao, G.J. Infiltration patterns and ecological function of outcrop runoff in epikarst areas of southern China. *Vadose Zone J.* **2018**, *17*, 170197. [CrossRef]
38. Canton, Y.; Rodríguez-Caballero, E.; Contreras, S.; Villagarcia, L.; Li, X.Y.; Solé-Benet, A.; Domingo, F. Vertical and lateral soil moisture patterns on a Mediterranean karst hillslope. *J. Hydrol. Hydromech.* **2016**, *64*, 209. [CrossRef]
39. Li, Y.; Zhou, Q.W.; Zhao, Y.L.; Cai, L.L.; Li, K.P.; Chen, Z.S.; Guo, Q. Regulation of shallow soil hydrological processes by rainfall characteristics and vegetation type on karst hillslopes: Insights from plot-scale field experiments. *J. Hydrol.* **2025**, *663*, 134199. [CrossRef]
40. Yang, X.; Zhang, K.; Shaghaleh, H.; Qi, Z.; Gao, C.; Chang, T.; Zhang, J.; Zia-ur-Rehman, M.; Hamoud, Y.A. Continuous cropping alters soil hydraulic and physicochemical properties in the karst region of southwestern China. *Agronomy* **2023**, *13*, 1416. [CrossRef]
41. Estrada-Medina, H.; Graham, R.C.; Allen, M.F.; Jiménez-Osornio, J.J.; Robles-Casolco, S. The importance of limestone bedrock and dissolution karst features on tree root distribution in northern Yucatán, México. *Plant Soil* **2013**, *362*, 37–50. [CrossRef]
42. Fan, C.H.; Zhao, L.S.; Hou, R.; Fang, Q.; Zhang, J.X. Quantitative analysis of rainwater redistribution and soil loss at the surface and belowground on karst slopes at the microplot scale. *Catena* **2023**, *227*, 107113. [CrossRef]
43. Hofierka, J.; Gallay, M.; Bandura, P.; Sasak, J. Identification of karst sinkholes in a forested karst landscape using airborne laser scanning data and water flow analysis. *Geomorphology* **2018**, *308*, 265–277. [CrossRef]
44. Chen, H.S.; Hu, K.; Nie, Y.P.; Wang, K.L. Analysis of soil water movement inside a footslope and a depression in a karst catchment, Southwest China. *Sci. Rep.* **2017**, *7*, 2544. [CrossRef] [PubMed]
45. Wang, Z.H.; Luo, D.; Xiong, K.N.; Gu, X.; Zhu, Z.Z. Studies on hydrological processes on karst slopes for control of soil and water loss. *Sustainability* **2022**, *14*, 5789. [CrossRef]
46. Yan, Y.J.; Dai, Q.H.; Jin, L.; Wang, X.D. Geometric morphology and soil properties of shallow karst fissures in an area of karst rocky desertification in SW China. *Catena* **2019**, *174*, 48–58. [CrossRef]
47. Wang, S.; Yan, Y.; Zhao, Y.J.; Fu, Z.Y.; Chen, H.S. Co-evolution among soil thickness, epikarst weathering degree, and runoff characteristics on a subtropical karst hillslope. *J. Hydrol.* **2024**, *628*, 130499. [CrossRef]
48. Zhang, Z.M.; Huang, X.F.; Zhang, J.C. Soil thickness and affecting factors in forestland in a karst basin in Southwest China. *Trop. Ecol.* **2020**, *61*, 267–277. [CrossRef]
49. Zhang, J.; Wang, S.; Fu, Z.Y.; Chen, H.S.; Wang, K.L. Soil thickness controls the rainfall-runoff relationship at the karst hillslope critical zone in southwest China. *J. Hydrol.* **2022**, *609*, 127779. [CrossRef]
50. Hou, F.; Cheng, J.H.; Guan, N. Investigating the effect of soil cracks on preferential flow using a dye tracing infiltration experiment in karst in Southwest China. *Land Degrad. Dev.* **2023**, *34*, 1612–1628. [CrossRef]
51. Li, M.; Wang, K.; Ma, X.; Fan, M.; Song, Y. Effects of land use change on soil aggregate stability and erodibility in the karst region of southwest China. *Agronomy* **2024**, *14*, 1534. [CrossRef]

52. Fu, Z.Y.; Chen, H.S.; Xu, Q.X.; Jia, J.T.; Wang, S.; Wang, K.L. Role of epikarst in near-surface hydrological processes in a soil mantled subtropical dolomite karst slope: Implications of field rainfall simulation experiments. *Hydrol. Process.* **2016**, *30*, 795–811. [CrossRef]
53. Hou, F.; Cheng, J.H.; Zhang, H.; Wang, X.L.; Shi, D.W.; Guan, N.; Yu, Y. Effects of geological features on preferential flow on karst slopes in southwestern China. *Earth Surf. Proc. Land.* **2025**, *50*, e70018. [CrossRef]
54. Duan, X.Q.; Fu, Z.Y.; Deng, Y.S.; Chen, H.S. Characteristics of water distribution and preferential flow processes and nutrient response on dolomite slopes in the southwestern karst region. *Front. Environ. Sci.* **2025**, *12*, 1511449. [CrossRef]
55. Guan, N.; Cheng, J.H.; Shi, X.Q. Preferential flow and preferential path characteristics of the typical forests in the karst region of southwest China. *Forests* **2023**, *14*, 1248. [CrossRef]
56. Wei, H.; Yang, Y.F.; Wang, J.Y.; Meng, Q.M.; Deng, Y.S. A comparison of preferential flow characteristics and influencing factors between two soils developed in the karst region of Southwest China. *Soil Till. Res.* **2024**, *241*, 106132. [CrossRef]
57. Liu, C.N.; Huang, Y.; Wu, F.; Liu, W.J.; Ning, Y.Q.; Huang, Z.R.; Tang, S.Q.; Liang, Y. Plant adaptability in karst regions. *J. Plant Res.* **2021**, *134*, 889–906. [CrossRef] [PubMed]
58. Wei, X.C.; Zhou, Q.W.; Luo, Y.; Cai, M.Y.; Zhou, X.; Yan, W.H.; Peng, D.W.; Zhang, J. Vegetation dynamics and its response to driving factors in typical karst regions, Guizhou Province, China. *Front. Earth Sci.* **2021**, *15*, 167–183. [CrossRef]

Disclaimer/Publisher's Note: The statements, opinions and data contained in all publications are solely those of the individual author(s) and contributor(s) and not of MDPI and/or the editor(s). MDPI and/or the editor(s) disclaim responsibility for any injury to people or property resulting from any ideas, methods, instructions or products referred to in the content.